



Retrieval of cloud properties from near-ultraviolet, visible, and near-infrared satellite-based Earth reflectivity spectra: A comparative study

R. van Deelen,¹ O. P. Hasekamp,¹ B. van Dierenhoven,¹ and J. Landgraf¹

Received 4 July 2007; revised 8 January 2008; accepted 28 February 2008; published 19 June 2008.

[1] In this study, we investigate the capability to retrieve cloud parameters from near-ultraviolet, visible, and near-infrared satellite-based reflectivity measurements. These parameters are essential to enable trace gas retrievals for cloud-contaminated satellite scenes. We compare the retrieval of cloud top pressure, cloud fraction, and cloud optical thickness from simulated reflectivity measurements in three wavelength ranges: (1) 350–400 nm, which includes pronounced Ring effect structures; (2) 460–490 nm; and (3) 755–775 nm, which contain absorption features of O₂-O₂ and O₂, respectively. Retrieval simulations are performed for both a typical noise level of present-day space-borne spectrometers and additional random-like measurement biases. Furthermore, we investigated the importance of the spectral continuum for the retrieval of cloud properties. It is found that reflectivity measurements in the wavelength ranges 350–400 and 755–775 nm provide complementary information on cloud properties. Both spectral windows provide more information on clouds than the 460–490 nm window. The best results are obtained for the combination of the 350–400 and 755–775 nm windows. In this case all three cloud parameters can be retrieved independently, and a high robustness is obtained with respect to random-like measurement biases. Here it is not required to resolve the Ring effect structures in the near-ultraviolet window. For this combination of spectral windows the error on retrieved NO₂ columns is reduced considerably.

Citation: van Deelen, R., O. P. Hasekamp, B. van Dierenhoven, and J. Landgraf (2008), Retrieval of cloud properties from near-ultraviolet, visible, and near-infrared satellite-based Earth reflectivity spectra: A comparative study, *J. Geophys. Res.*, *113*, D12204, doi:10.1029/2007JD009129.

1. Introduction

[2] Satellite instruments that measure Earth reflectivity spectra in the near-ultraviolet (NUV), visible (VIS), and near-infrared (NIR) wavelength range are used to monitor important atmospheric constituents on a global scale, e.g., ozone (O₃), water vapor (H₂O), nitrogen dioxide (NO₂), and aerosols. Examples of such instruments are the first and second Global Ozone Monitoring Experiment (GOME and GOME-2) [Burrows *et al.*, 1999b; Callies *et al.*, 2000], which cover the spectral range 240–790 nm with a spectral resolution of 0.17–0.35 nm and 0.22–0.53 nm, respectively. Furthermore, the Scanning Imaging Absorption Spectrometer for Atmospheric Chartography (SCIAMACHY) [Bovensmann *et al.*, 1999] observes the spectral range 220–2400 nm with a spectral resolution 0.22–1.50 nm. The Ozone Monitoring Experiment (OMI) [Levelt *et al.*, 2006] has a reduced spectral coverage of 270–500 nm with a spectral resolution of 0.45–1.00 nm. The size of the ground scene that is observed by these satellite instruments differs considerably. The area is largest for GOME with

320 × 40 km² (across × along track) and smallest for OMI with 24 × 13 km². Because these satellite instruments have a large field of view, nearly all observations contain clouds: more than 94% for GOME, SCIAMACHY, and GOME-2, and approximately 88% for OMI [Krijger *et al.*, 2007]. Clouds strongly affect the light paths of solar radiation through the atmosphere and change the air masses that are seen by the measured radiation. In order to determine trace gas concentrations as accurately as possible, cloud parameters are required that adequately describe the measured reflectivity spectra in cloudy conditions [e.g., Koelemeijer and Stammes, 1999; Wang *et al.*, 2006]. Since clouds are highly variable in space and time, the cloud parameters are preferably derived from the same reflectivity spectrum that is used for the trace gas retrieval. This is done to guarantee collocation in space and time of both the cloud parameters and the retrieved atmospheric trace gases.

[3] A well established method to retrieve cloud parameters from reflectivity measurements is to use absorption bands of molecular oxygen (O₂) [Daniel *et al.*, 2003] of which the vertical distribution is accurately known. The oxygen A (O₂ A) band near 760 nm is often selected [Kuze and Chance, 1994; Koelemeijer *et al.*, 2001]. These measurements are provided by GOME, SCIAMACHY, and GOME-2. The OMI instrument lacks the O₂ A band and

¹Netherlands Institute for Space Research, Utrecht, Netherlands.

therefore the much weaker absorption line of collision complexes of oxygen (O_2-O_2) at 477 nm is used instead [Daniel *et al.*, 2003; Acarreta *et al.*, 2004]. The O_2 density is sufficiently high in the lower part of the Earth's atmosphere for radiation to be absorbed during the short time interval that two colliding O_2 molecules form an O_2-O_2 dimer. A third method makes use of the Ring effect in the NUV wavelength range [Grainger and Ring, 1962; Joiner *et al.*, 1995; de Beek *et al.*, 2001; Joiner and Vasilkov, 2006]. This effect is caused by rotational Raman scattering by nitrogen (N_2) and oxygen (O_2) molecules. This inelastic scattering of sunlight decreases the depth of Fraunhofer lines in an Earth radiance spectrum, which is also known as filling in. The presence of cloud and aerosol particles, which scatter solar radiation elastically, alters the probability that radiation is scattered inelastically. As a consequence, the filling in is different compared to the clear-sky case [Joiner *et al.*, 1995; de Beek *et al.*, 2001; Stam *et al.*, 2002]. Furthermore, van Diedenhoven *et al.* [2007] showed that combining reflectivity spectra of the O_2 A absorption band and reflectivity measurements in the wavelength range 350–390 nm leads to an improved retrieval of cloud properties. The combination of the NUV and NIR reflectivity measurements leads to an improved retrieval of cloud properties and has been successfully applied to GOME measurements. However, the additional cloud information that is contained in the Ring effect was not exploited in their approach, since the Ring effect was partially removed by fitting precalculated Ring structures.

[4] Because of the different possible retrieval concepts, the question is raised which spectral range or which combination of spectral ranges is most suited for an appropriate retrieval of cloud parameters from measurements as performed by GOME. In this work, we compare the capability to retrieve cloud parameters from (combinations of) three wavelength ranges: (1) 350–400 nm, hereafter referred to as the NUV window, which contains pronounced Ring effect structures and two weak O_2-O_2 absorption bands, (2) 460–490 nm, hereafter referred to as the VIS window, which contains a stronger absorption band of O_2-O_2 , and (3) 755–775 nm, hereafter referred to as the NIR window, which contains the O_2 A band. Our work can be viewed as an extension of the comparative study of Daniel *et al.* [2003] who considered the retrieval capability of several O_2 absorption bands, O_2-O_2 absorption bands, and combinations hereof. We include the NUV window and study the added value of the Ring effect in cloud parameter retrievals.

[5] We use the following approach: First, we simulate reflectivity spectra of cloudy scenes that are characterized by three cloud parameters: cloud top pressure, cloud fraction, and cloud optical thickness. The ground surface albedo is fitted as an additional parameter. Next we determine the cloud parameters and the surface albedo from the synthetic measurements as a function of measurement noise and cloud fraction. This analysis is performed for the spectral windows separately and for combinations of the spectral windows. Since satellite-based Earth reflectivity spectra are often subject to significant radiometric calibration errors, it is common to use only spectral features of the measurement which are defined relative to broadband spectral structures. In this way, the sensitivity to broadband calibration errors

can generally be reduced, but potential information that is present in the broadband continuum of the measurement is not exploited. We therefore choose to investigate two additional scenarios: (1) when only the spectral features relative to the reflectivity continuum spectrum are used, and (2) when all spectral features except the absolute values of the reflectivity continuum are used (i.e., the spectral signature of the continuum is included, but not the continuum height). The comparison of the cloud parameter retrieval from the different spectral windows is not only relevant for the data analysis of reflectivity spectra measured by present-day satellite instruments, but also for decisions on the optimal design of future space-borne spectrometers. For future missions to monitor air quality from space, which are currently under assessment, it is important to minimize the spectral coverage of the involved spectrometers and to optimize the retrieval of cloud parameters, which are required to retrieve tropospheric trace gas abundances. This raises two important questions: Firstly, is it needed to measure reflectivity spectra in the spectral range of the O_2 A band, and secondly, what is the added value of the Ring effect in the NUV spectral range?

[6] The paper is constructed as follows: In section 2, the forward model is described. In section 3, the sensitivity of GOME-type measurements to cloud properties and the role of the spectral continuum, the Ring effect structures, and absorption features are explained for the different spectral windows. In section 4, we describe the inversion scheme that is used to retrieve cloud parameters from simulated measurements. In section 5, the retrieval capabilities of the three selected spectral windows are assessed separately, whereas in section 6 combinations of spectral windows are investigated. In section 7 we discuss how retrieval errors on the cloud parameters affect the retrieval of tropospheric NO_2 columns. We end with a summary in section 8.

2. Forward Model

[7] The reflectivity of the Earth's atmosphere and surface is defined as $r = \pi I / (\mu_0 F)$, where I is the intensity that is reflected by the Earth, F is the daily measured solar irradiance, and μ_0 is the cosine of the solar zenith angle. For the simulation of cloudy reflectivity measurements a model is required that describes the most relevant effects of clouds on r . Several recently developed models describe clouds as a scattering layer [Ahmad *et al.*, 2004; Liu *et al.*, 2004; van Diedenhoven *et al.*, 2006; de Beek *et al.*, 2001] in which cloud optical thickness is used as an important cloud parameter. To circumvent time-consuming radiative transfer calculations, other schemes are used that simplify clouds as an elevated Lambertian reflector with a given Lambertian cloud albedo [e.g., Joiner *et al.*, 2004; Koelmeijer *et al.*, 2001]. In this paper we choose to simulate the cloud as an elevated reflecting surface of which the reflectivity is a function of optical thickness. We adopted the bidirectional reflection function (BDRF) of Kokhanovsky *et al.* [2003] for this purpose. This BDRF, which was derived from the asymptotic theory of radiative transfer, represents the reflection by an idealized semi-infinite nonabsorbing cloud. It is valid for water clouds with an optical thickness ≥ 5 , which limits our study to these cloud types. In addition, we ignore three-dimensional radiative transfer effects and thus

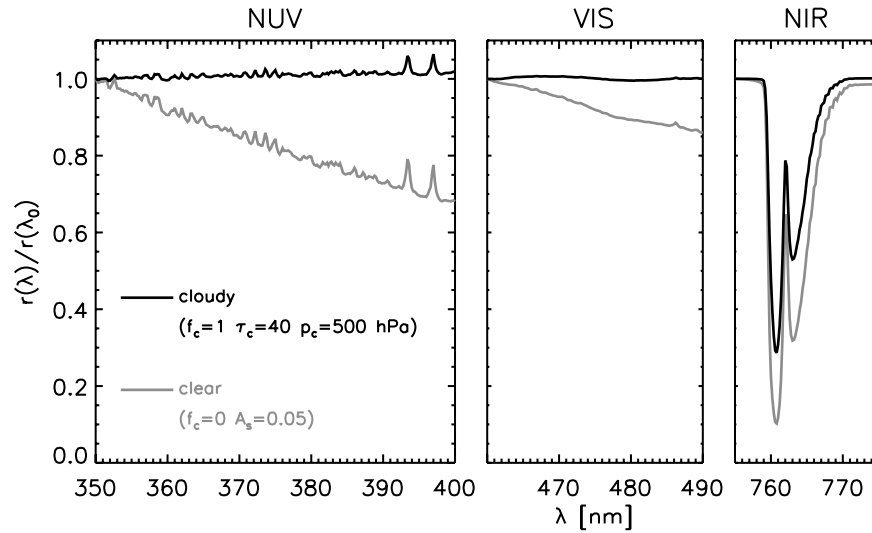


Figure 1. Reflectivity spectra of a clear-sky observation (gray curve, $f_c = 0$ and $A_s = 0.05$) and a fully cloudy observation (black curve, $f_c = 1$, $\tau_c = 40$, and $p_c = 500$ hPa) in the NUV, VIS, and NIR wavelength ranges normalized to their reflectivity value at the start of each wavelength interval. For the NUV, VIS, and NIR windows these values are $r(\lambda_0) = 0.25, 0.12, 0.06$ and $0.78, 0.80, 0.82$ for the cloud-free scene and fully cloudy scene, respectively. A nadir viewing geometry and a solar zenith angle of 40° were used.

the independent pixel approximation can be used [see, e.g., Marshak *et al.*, 1999]. The reflectivity of a cloudy scene is then simulated as

$$r(p_c, f_c, \tau_c, A_s) = f_c r_{\text{cld}}(p_c, \tau_c) + [1 - f_c] r_{\text{clr}}(A_s). \quad (1)$$

Here, r_{cld} and r_{clr} represent the reflectivity for the cloudy part and the clear-sky part of the observed scene, respectively. A fraction f_c of the observed satellite scene is covered by a cloud with a certain optical thickness τ_c and a certain cloud top pressure p_c . The remaining part of the scene is considered cloud free with a Lambertian reflecting surface (surface albedo A_s) at the ground. Other parameters than p_c, f_c, τ_c , and A_s , such as surface pressure, are assumed to be known a priori.

[8] To simulate the reflectivity in equation (1) we used the plane-parallel vector radiative transfer model of Landgraf *et al.* [2004]. This model includes polarization and one order of rotational Raman scattering. For this study, we convoluted the simulated reflectivity spectrum with a Gaussian slit function with a full width at half maximum of 0.2 nm in the NUV window, of 0.3 nm in the VIS window, and of 0.4 nm in the NIR window. The smoothed spectra were subsequently sampled at spectral sampling intervals of 0.2 nm. Furthermore, we assumed a polarization insensitive instrument in the simulation. These choices represent a compromise between the different spectral characteristics of the GOME, GOME-2, SCIAMACHY and OMI instruments.

[9] The plane-parallel model atmosphere is based on the U.S. Standard Atmosphere (1976) and is subdivided into 1-km thick layers for the lowest 10 km and 2-km layers for higher altitudes. The scattering properties of air are calculated using data provided by Bates [1984], Peck and Fisher [1964] and Pennney *et al.* [1974] (see Landgraf *et al.* [2004] for more details). The absorption cross sections of O_2 and

H_2O are taken from the HITRAN2004 database [Rothman *et al.*, 2005]; those of O_3 are adopted from Burrows *et al.* [1999a]; the absorption cross sections of NO_2 are taken from Vandaele *et al.* [1998]; and those of $\text{O}_2\text{-O}_2$ at 360 nm, 380 nm and 477 nm are taken from Greenblatt *et al.* [1990]. Absorption by other gases is assumed to be insignificant.

[10] The effect of inelastic Raman scattering on a reflectivity spectrum is commonly described by a filling in or Ring spectrum, defined as

$$R(\lambda) = \frac{I_{\text{ram}}(\lambda) - I_{\text{ray}}(\lambda)}{I_{\text{ray}}(\lambda)}. \quad (2)$$

Here, $I_{\text{ray}}(\lambda)$ represents an intensity spectrum of reflected light that is simulated using the Rayleigh scattering approximation (i.e., all scattering is assumed to be elastic), and $I_{\text{ram}}(\lambda)$ denotes the intensity spectrum that takes inelastic Raman scattering into account. The deviation of the Ring spectrum from zero is called the Ring effect [e.g., Joiner *et al.*, 1995]. This effect is most prominent in the ultraviolet wavelength range where scattering by molecules is strong and where many Fraunhofer lines are present. The filling in of the O_2 A band is of minor importance for GOME(-2) and SCIAMACHY measurements [Sioris and Evans, 2000]. Therefore, we adopt the Rayleigh scattering approximation in the NIR window, which simplifies the radiative transfer model considerably.

3. Sensitivity of Measurement to Cloud Properties

[11] The reflectivity spectrum can be dissected into three spectral components that are sensitive to cloud properties: (1) the spectral continuum, (2) the Ring spectrum, and (3) molecular absorption features. The relative importance of each spectral component is different for the NUV, VIS, and NIR window. Figure 1 shows a simulated reflectivity

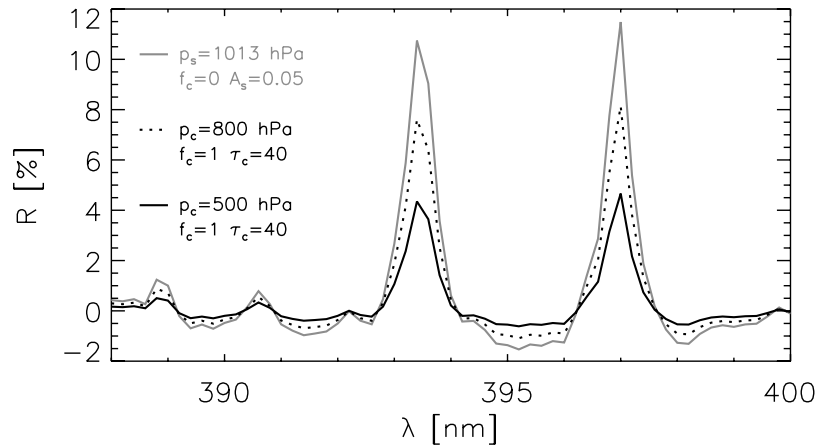


Figure 2. Ring spectra in the wavelength range 388–400 nm for a clear-sky observation (gray curve, $f_c = 0$ and $A_s = 0.05$; surface pressure $p_s = 1013$ hPa) and for two fully cloudy observations (black curves, $f_c = 1$ and $\tau_c = 40$) with different cloud top height. Increasing the cloud top height from 1.9 km ($p_c = 800$ hPa, dotted line) to 5.6 km altitude ($p_c = 500$ hPa, black solid line) leads to a reduction of the Ring effect structures. We used the solar spectrum of *Chance and Spurr* [1997] as input for our simulations.

spectrum r for a clear-sky scene ($A_s = 0.05$) and a fully cloud covered scene ($p_c = 500$ hPa, $f_c = 1$, $\tau_c = 40$) normalized to the reflectivity value at the shortest wavelength of each wavelength interval. For all three spectral windows, the clear-sky reflectivity r_{clr} decreases toward longer wavelengths. This property of the spectral continuum is a direct consequence of molecular scattering with a scattering cross section proportional to λ^{-4} [e.g., *Bucholtz, 1995*]. At shorter wavelengths more solar radiation is scattered into the satellite instrument's line of sight than at longer wavelengths. For fully cloud covered scenes hardly any wavelength dependence of the reflectivity continuum spectrum is observed. Here, the wavelength independent reflection of the bright cloud surface overwhelms the contribution of atmospheric scattering. For the NUV window, and to a lesser degree for the VIS window, this results even in a small increase of the reflectivity toward longer wavelengths. The atmosphere is optically more dense at shorter wavelengths because of stronger molecular scattering. As a consequence, less light that has been reflected by the cloud emerges from the atmosphere into direction of the satellite instrument at the shorter wavelengths. The wavelength dependence of the continuum is most pronounced in the NUV and VIS windows. Therefore it is expected that the reflectivity spectra at these wavelengths provide a clear sensitivity to cloud properties. In sections 5 and 6, the importance of the spectral continuum for the retrieval of cloud parameters is investigated.

[12] Secondly, the Ring spectrum is affected by clouds. The Ring effect is explained by inelastic scattering by air that effectively transfers light from the wings of the Fraunhofer lines to their line centers. This results in an enhanced reflectivity at the center of a Fraunhofer line and a reduced reflectivity at the wings. The strength of the Ring effect depends on the depth and shape of each Fraunhofer line and on the relative amount of measured photons that are inelastically scattered compared to those that are elastically scattered. In the case of a cloudy atmosphere less light is scattered by air molecules than in a cloud-free atmosphere,

which results generally in less pronounced Ring spectra in cloudy observations. The sensitivity of the Ring spectrum to clouds is highest for the spectral range where the strongest filling-in features exist, i.e., at the Ca II K and H lines near 393.4 and 397.0 nm. Figure 2 shows that the filling in of these Fraunhofer lines can reach 11% for a clear-sky scene in nadir viewing geometry and a solar zenith angle of 40° . For a low cloud at 800 hPa the filling in is reduced to 8%, and for a higher cloud at 500 hPa it is reduced further to approximately 4%. An important goal of this study is to investigate the relevance of inelastic Raman scattering for cloud parameter retrievals from measurements in the NUV spectral window. In the other selected windows the Ring spectra are very weak and are thus not considered.

[13] Additionally, the reflectivity measurement is sensitive to clouds because of absorption lines of molecular oxygen. The most prominent absorption feature of O_2 is located in the NIR window. Another significant but much weaker absorption band is the $\text{O}_2\text{-O}_2$ absorption band in the VIS window. A large part of the sensitivity to clouds arises from the shielding effect of clouds; the vertical column of O_2 and $\text{O}_2\text{-O}_2$ below the cloud is shielded and hence the depths of the O_2 and $\text{O}_2\text{-O}_2$ absorption features are reduced. Since the total amount of O_2 in the atmosphere is known, the reduced depth of the O_2 and $\text{O}_2\text{-O}_2$ absorption features can be related to cloud height.

[14] To summarize, the sensitivity of the measurement in the NUV window with respect to cloud parameters is mainly determined by the spectral continuum and the Ring features. The measurement in the VIS window is sensitive to cloud parameters because of the spectral continuum contribution and atmospheric absorption by $\text{O}_2\text{-O}_2$. In the NIR spectral range the absorption of O_2 is the most relevant spectral feature. This means that the sensitivity of the reflectivity measurement to clouds originates from different spectral components of the reflectivity spectrum in each spectral range. This makes it interesting to compare the retrieval capability of measurements in the different spectral ranges. For this purpose we perform retrievals from simu-

lated reflectivity measurements from the NUV, VIS, and NIR windows, and from combinations of those.

4. Inversion and Retrieval Diagnostics

[15] To determine the cloud parameters from reflectivity measurements we assume that a forward model \mathbf{F} describes the measurement vector \mathbf{y} as a function of the atmospheric state vector \mathbf{x} as

$$\mathbf{y} = \mathbf{F}(\mathbf{x}) + \mathbf{e}_y, \quad (3)$$

where \mathbf{e}_y is the measurement error vector. We assume that the components of \mathbf{e}_y are uncorrelated, and thus, the measurement error covariance matrix \mathbf{S}_y is given by a diagonal matrix that has the variance of the measurement error on its diagonal. In our case, the measurement vector \mathbf{y} contains the reflectivity spectrum for the different spectral ranges, and the state vector is given by $\mathbf{x} = [p_c, f_c, \tau_c, A_s]^T$. Here, T stands for the transpose of the vector.

[16] The state vector \mathbf{x} has to be determined by inverting equation (3). Since the forward model is nonlinear in the unknown parameters, an iterative scheme has to be used to find the solution of the inverse problem. For each iteration step, the forward model is replaced by its linear approximation around the vector \mathbf{x}_n of the previous iteration step n ,

$$\mathbf{F}(\mathbf{x}) \approx \mathbf{F}(\mathbf{x}_n) + \mathbf{K}[\mathbf{x} - \mathbf{x}_n]. \quad (4)$$

Here, \mathbf{K} is the Jacobian matrix that contains the derivatives of the forward model with respect to the elements of \mathbf{x}_n . Each element K_{ij} is defined by

$$K_{ij} = \frac{\partial F_i}{\partial x_j}(\mathbf{x}_n). \quad (5)$$

These derivatives indicate the measurement sensitivity to the parameters x_j .

[17] For the three selected windows, the satellite measurements generally do not contain sufficient information to retrieve all four parameters p_c, f_c, τ_c , and A_s independently. This means that many combinations of parameters exist that fit the measured reflectivity spectrum (almost) equally well. In this case, the inversion problem is ill posed and the least squares solution of the inversion problem is overwhelmed by noise. Regularization is required to obtain a stable solution. In this study, we adopt the Tikhonov regularization method [Phillips, 1962; Tikhonov, 1963] as it is described by Hasekamp and Landgraf [2005]. This method introduces a side constraint in addition to the minimization of the least squares residual norm. As a side constraint, we choose the minimization of a weighted norm of the state vector. So the regularized least squares solution \mathbf{x}_{reg} becomes

$$\mathbf{x}_{\text{reg}} = \min_{\mathbf{x}} \left(\|\mathbf{S}_y^{-1/2}(\mathbf{F}(\mathbf{x}) - \mathbf{y})\|^2 + \gamma \|\Gamma \mathbf{x}\|^2 \right), \quad (6)$$

where Γ is a diagonal matrix that contains weight factors for the different elements of the state vector. Here, the weighting factors are chosen as $\Gamma_i = 1/x_{a,i}$, where $x_{a,i}$ are the elements of an a priori state vector \mathbf{x}_a . The regularization parameter γ balances the two contributions in equation (6)

and determines the amount of information that is extracted from the measurements. For each retrieval an appropriate value of γ is found by the L curve method [Hansen, 1992; Hansen and O'Leary, 1993].

[18] The regularized solution of equation (6) is given by

$$\mathbf{x}_{\text{reg}} = \mathbf{D}\tilde{\mathbf{y}}, \quad (7)$$

with $\tilde{\mathbf{y}} = \mathbf{y}_{\text{meas}} - \mathbf{F}(\mathbf{x}_n) + \mathbf{K}\mathbf{x}_n$, and with the contribution matrix

$$\mathbf{D} = \left(\mathbf{K}^T \mathbf{S}_y^{-1} \mathbf{K} + \gamma \Gamma \right)^{-1} \mathbf{K}^T \mathbf{S}_y^{-1}. \quad (8)$$

The regularized state vector is a weighted average of the true state vector,

$$\mathbf{x}_{\text{reg}} = \mathbf{A}\mathbf{x}_{\text{true}} + \mathbf{e}_x. \quad (9)$$

Here, \mathbf{A} is the so-called averaging kernel of the inversion and is given by

$$\mathbf{A} = \mathbf{D}\mathbf{K}, \quad (10)$$

and \mathbf{e}_x is the retrieval noise, which is the error on the state vector as a result of the measurement noise. The retrieval noise on the different parameters, $e_{x,i}$, can be quantified by taking the square root of the diagonal elements of the retrieval noise covariance matrix:

$$\mathbf{S}_x = \mathbf{D}\mathbf{S}_y\mathbf{D}^T. \quad (11)$$

[19] The retrieval capability of a given measurement can be assessed by analyzing the elements of the averaging kernel \mathbf{A} . The degree of smoothing of the averaging kernel in equation (9) reflects the degree of regularization that is needed to stabilize the inversion. For our purpose it suffices to focus on the diagonal elements of the averaging kernel only,

$$C_i = A_{ii} = \frac{\partial x_{\text{reg},i}}{\partial x_{\text{true},i}}, \quad (12)$$

which indicate how much the regularized value $x_{\text{reg},i}$ depends on the true parameter $x_{\text{true},i}$. Hereafter, this quantity C_i is referred to as the retrieval sensitivity. In case of a well-posed problem, $C_i = 1$ for each parameter x_i and so all parameters can be retrieved independently. If the retrieval is not sensitive at all to a certain parameter, then $C_i = 0$. This makes C_i a useful diagnostic tool to study the capabilities of the different spectral windows to retrieve information on the cloud parameters p_c, f_c, τ_c , and on the surface albedo A_s in each window. The sum of the retrieval sensitivities of all parameters; that is, $\sum_i C_i$, is known as the degrees of freedom for signal [Rodgers, 2000]. It denotes the number of independent pieces of information that can be retrieved from the measurement.

[20] When using the retrieved cloud parameters for trace gas retrievals it is important to realize that the regularized state vector \mathbf{x}_{reg} does not provide a physical solution of the problem, but presents a weighted average of the elements of

the physical state. To obtain a physical solution, one has to add a priori information to the regularized state vector \mathbf{x}_{reg} as

$$\hat{\mathbf{x}} = \mathbf{x}_{\text{reg}} + (\mathbf{I} - \mathbf{A})\mathbf{x}_a, \quad (13)$$

where \mathbf{x}_a is the a priori state vector with an a priori error covariance matrix \mathbf{S}_a . The error on the retrieval result $\hat{\mathbf{x}}$ is given by the total error covariance matrix

$$\mathbf{S} = \mathbf{S}_x + \mathbf{S}_{\text{reg}}, \quad (14)$$

which equals the sum of the retrieval error covariance matrix \mathbf{S}_x in equation (11) and the regularization error covariance matrix

$$\mathbf{S}_{\text{reg}} = (\mathbf{I} - \mathbf{A})\mathbf{S}_a(\mathbf{I} - \mathbf{A})^T. \quad (15)$$

5. Information Content of the NUV, VIS, and NIR Spectral Window

[21] The instrument noise on GOME, GOME-2, SCIAMACHY, and OMI measurements is of the order of 0.1% in the NUV, VIS, and NIR wavelength ranges. In practice, the differences between modeled and measured reflectivity spectra are a few times larger than this instrument noise level and appear random [e.g., Joiner et al., 2004; van Deelen et al., 2007; van Diedenhoven et al., 2007]. The origin of these large residuals can be manifold, e.g., problems in the instrument calibration, errors in the simulation of the measurements, and uncertainties in spectroscopic data such as the O₂ A band cross sections [Rothman et al., 2005] and line shapes [Yang et al., 2005; Tran et al., 2006]. The existence of these possible sources of error makes it useful to study the robustness of the retrieval to random-like biases on top of the instrument noise.

[22] Figure 3 shows the retrieval sensitivities C_{pc} , C_{fc} , and C_{τ_c} as a function of a white noise floor η that is added to the instrument noise of 0.1% for the three spectral windows. All curves in Figure 3 were calculated for a fully cloudy scene ($f_c = 1$). In general, the retrieval sensitivities decrease when η is increased, because the effect of clouds on the signature of the spectral continuum and on the spectrally fine structures becomes more difficult to distinguish from noise. For example, the retrieval sensitivity C_{pc} for the NUV window decreases from $C_{pc} \approx 1$ at $\eta = 0\%$ to $C_{pc} \approx 0.3$ at $\eta = 1.5\%$ for a high and optically thick cloud ($p_c = 500$ hPa, $\tau_c = 40$). In case of a low and optically thin cloud ($p_c = 800$ hPa, $\tau_c = 5$) this loss in retrieval sensitivity is less: C_{pc} is still larger than 0.9 at $\eta = 1.5\%$. For the VIS window increasing the noise floor has a stronger impact than for the other windows because the cloud sensitive spectral features are weaker in this window. Here, the retrieval sensitivity C_{pc} decreases from $C_{pc} = 0.6$ at $\eta = 0\%$ to $C_{pc} < 0.3$ for noise floors larger than 1% for the high-cloud case. For low-cloud scenarios the sensitivity C_{pc} is significantly higher. This is explained by the quadratic dependence of the O₂-O₂ absorption optical depth on air density, which results in significantly weaker absorption at high altitudes in the troposphere than closer to the surface. The signature of the O₂-O₂ absorption features

relative to the noise is thus more rapidly lost for high clouds than for low clouds [Acarreta et al., 2004]. This situation is different for the cloud top pressure retrieval from the NIR window, which stays unaffected at noise levels even larger than 1%. The strong O₂ absorption feature dominates the reflectivity spectrum even in the case of very large noise levels.

[23] The retrieval sensitivity of cloud fraction shows a similar dependence on noise floor for all three spectral windows. For the VIS and NIR windows the sensitivity remains $C_{fc} \geq 0.9$ up to a $\eta = 1.5\%$ for an optically thick cloud, whereas for optically thinner clouds ($\tau_c = 5$ and 10) it decreases significantly with an increasing noise floor. Let us consider the retrieval of cloud optical thickness for the scenario $\tau_c = 40$. Here, the sensitivity $C_{\tau_c} \approx 0.8$ and $C_{\tau_c} \leq 0.5$ for the VIS and NIR windows respectively when no noise floor is added to the measurement simulation, whereas for $\eta = 0.5\%$ the sensitivity is reduced to $C_{\tau_c} \leq 0.1$. The retrieval of τ_c from the NUV window is far less sensitive to noise. Here, the retrieval sensitivity is 1 in case of no noise floor and larger than 0.6 for a noise floor of 0.5% for all cloud scenarios that are shown in Figure 3.

[24] For a proper interpretation of the retrieval sensitivity, one has to be sure that the changes in the retrieval sensitivity, and thus in the degree of regularization of the inversion problem, arise solely from differences in information that is present in the measurement. For this purpose we consider the retrieval noise $e_{x,i}$ in Figure 4 together with the retrieval sensitivity shown in Figure 3. In general, a higher retrieval sensitivity cannot automatically be associated with more information present in the measurement. It indicates a weaker regularization of the inversion and one has to make sure that a higher retrieval sensitivity is not accompanied by an enhanced retrieval error of the cloud parameters. In our case, Figure 4 shows that the retrieval noise $e_{x,i}$ for the different cloud parameters is of the same order of magnitude when we compare the different spectral windows. Only for the retrieval of cloud top pressure from the NIR window with a retrieval sensitivity close to 1 for the full range of noise floor values significantly lower retrieval errors are achieved. Overall, for a higher retrieval sensitivity we obtain a somewhat lower retrieval noise and vice versa. This clearly demonstrates that the variation of the retrieval sensitivities C_i in Figure 3 adequately reflects the retrieval capability of the different spectral windows.

[25] Summarized, for fully cloudy scenes it is possible to retrieve all three cloud parameters, p_c , f_c , and τ_c from the NUV window with sensitivities $C_i > 0.5$ up to reasonable noise levels (<0.8%). Of the three windows, the VIS window is most sensitive to additional random-like spectral biases on the measurement: here, the sensitivity to cloud top pressure retrieval for high clouds and to cloud optical thickness for thick clouds rapidly diminishes when the noise level increases to >0.5%. For low clouds though, the VIS window provides a similar performance as the NUV window. The retrieval of cloud top pressure from NIR window appears unaffected by noise floors up to 1.5%. The cloud optical thickness on the other hand (and to a lesser degree the cloud fraction retrieval) is highly sensitive to random-like biases.

[26] To investigate the retrieval capabilities of the NUV, VIS, and NIR windows in further detail, we choose a noise

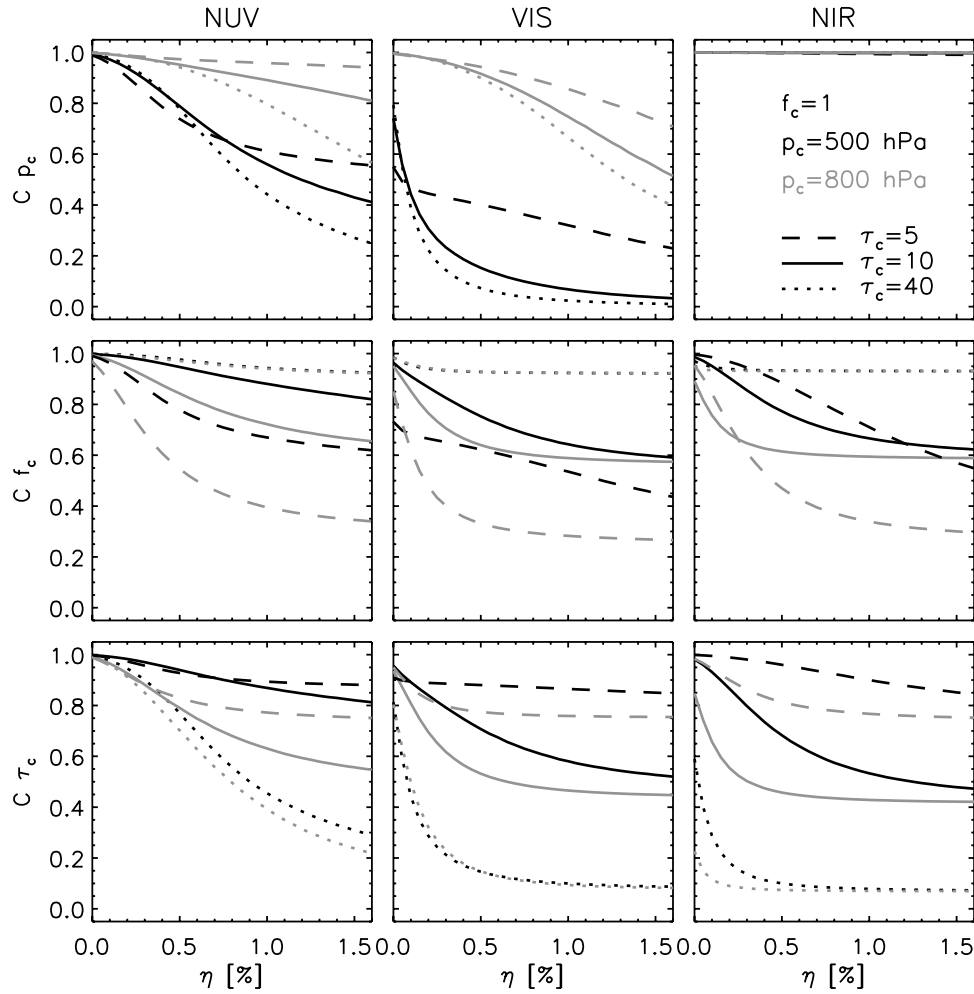


Figure 3. Retrieval sensitivities (C) to cloud top pressure (p_c), cloud fraction (f_c), and cloud optical thickness (τ_c) in the NUV, VIS, and NIR spectral windows as a function of the noise floor (η) that is added to the instrument noise of 0.1%. Results are shown for a fully cloudy scene ($f_c = 1$), and thus information on the surface albedo is absent. The dotted lines show the retrieval sensitivities for an optically thick cloud ($\tau_c = 40$), the solid lines for an optically thinner cloud ($\tau_c = 10$), and the dashed lines for an optically thin cloud ($\tau_c = 5$). The lines in gray correspond to a low cloud ($p_c = 800$ hPa) and the black lines to a high cloud at ($p_c = 500$ hPa). Note that the gray and black dotted lines for C_{f_c} versus η are on top of each other.

floor $\eta = 0.1\%$ and study the information on the cloud parameters as a function of cloud fraction. Figure 5 shows the sensitivity C_{p_c} , C_{f_c} , C_{τ_c} and C_{A_s} , as function of f_c . For the NUV window all three cloud parameters can be retrieved with a high sensitivity down to low-cloud fractions for nearly all scenarios. The situation differs for the VIS window where cloud top pressure retrieval shows a clearly lower retrieval sensitivity, e.g., $C_{p_c} \leq 0.45$ for the high-cloud scenario. As mentioned earlier this is caused by the weak O_2 - O_2 absorption coefficient at higher tropospheric altitudes. Finally, the NIR window provides highest-sensitivity $C_{p_c} \approx 1$ for the retrieval of p_c for all cloud fractions. However, it has its shortcoming in the retrieval of cloud optical thickness. For the optical thick cloud only a very low sensitivity is achieved of about $C_{\tau_c} = 0.1$ and also for optically thinner clouds the sensitivity does not exceed a value of 0.8 for cloud fractions $f_c < 0.5$. In all three spectral windows the Lambertian surface albedo can only be extracted from the

measurement when the cloud fraction is low. This holds for all cases that are studied in this paper and therefore the retrieval sensitivities C_{A_s} are hereafter not shown. Furthermore, we studied the retrieval noise e_x for the scenarios in Figure 5 (not shown). Similar to Figure 3 we found that the dependence of the retrieval noise on cloud fraction allows us, also in this case, to use the retrieval sensitivity to investigate cloud information in the measurement. This holds for the other scenarios in the remainder of this study as well.

[27] With the obtained results it is hard to identify one spectral window that has the best capability to retrieve all three cloud parameters. Cloud top pressure can be retrieved best using the NIR window but this spectral range has a lower retrieval sensitivity for f_c and τ_c . The latter two parameters can be retrieved from the NUV window with a high retrieval sensitivity. The VIS window shows weakest performance,

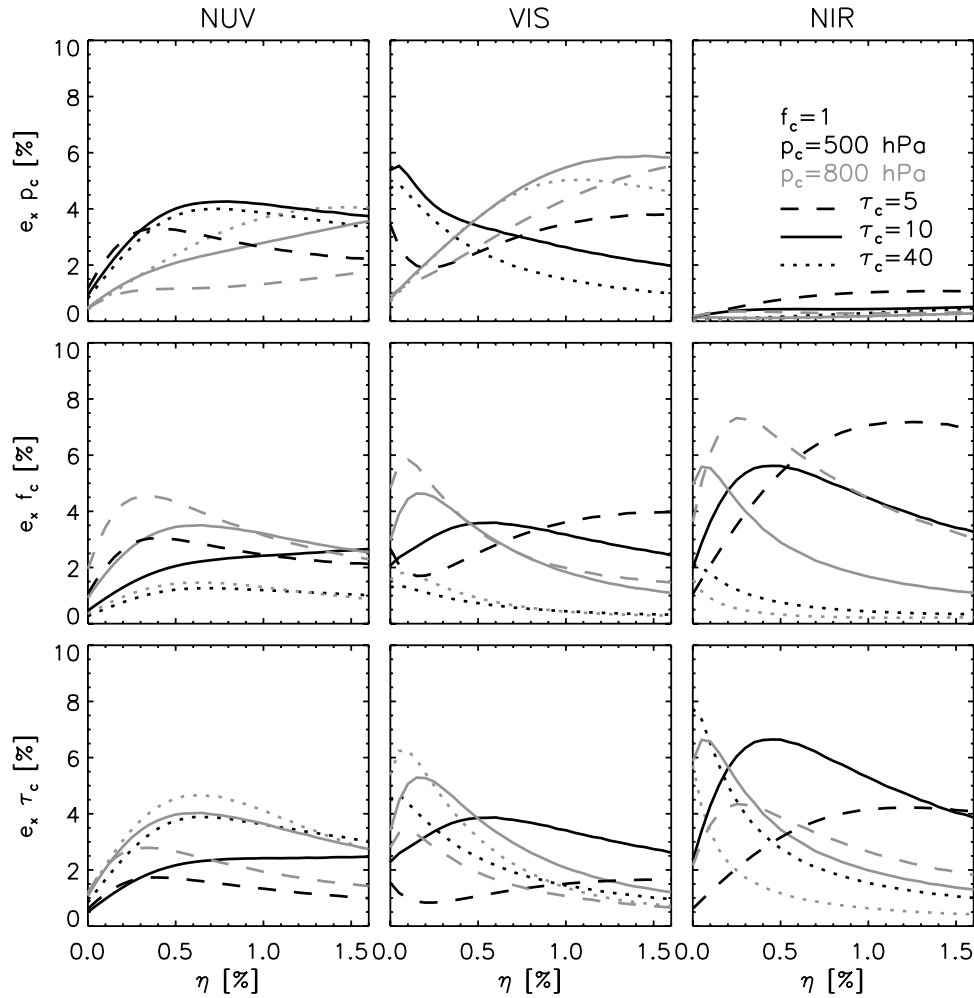


Figure 4. Same as Figure 3 but for retrieval noise (e_x ; see equation (11)) as function of noise floor (η).

especially for the high-cloud scenario for the retrieved p_c , and for optically thick clouds for the retrieved τ_c .

[28] A common approach in satellite remote sensing is to use only spectral structures relative to broadband spectral features of the measurement. For example, the differential optical absorption spectroscopy (DOAS) method uses this technique, which is employed in many trace gas retrieval applications in the ultraviolet, visible and near-infrared wavelength range [e.g., Platt, 1994]. One important advantage of this technique is its low sensitivity to broadband calibration errors of the measurement.

[29] For the retrieval of cloud properties we therefore consider two related approaches in this study. In the first approach we fit a scaling to the reflectivity measurement by adding the coefficients of a power law function

$$g(\lambda) = g_0(\lambda/\lambda_0)^\alpha \quad (16)$$

to the state vector. Here, g_0 represents the scaling ratio at a reference wavelength λ_0 of the spectral interval and the exponent α governs the wavelength dependence of the scaling factor. Thus the state vector that is to be retrieved is $\mathbf{x} = [p_c, f_c, \tau_c, A_s, g_0, \alpha]^T$. In the retrieval, the two parameters g_0 and α are given a strong weight (by setting $\Gamma_i = 10^8$ in equation (6)) to force that the scaling is fitted in any case.

Here, the function $g(\lambda)$ describes nearly all broadband spectral features of the reflectivity continuum in the three spectral windows. By adding g_0 and α to the state vector all information contained in the absolute value of the continuum as well as broad band features are eliminated.

[30] In a second approach we add only a wavelength independent scaling factor g_0 to the state vector. In contrast to the first approach, this will allow information to be extracted from the broad band features present in the window. The comparison of the retrieval sensitivity of both approaches with those where all spectral information of the reflectivity spectrum is used allows us to investigate the importance of the spectral continuum for the retrieval of cloud properties versus the importance of the differential Ring and absorption structures alone.

[31] Figure 6 shows C_{p_c} , C_{f_c} , and C_{τ_c} as function of cloud fraction for both scaling factor scenarios (approach 1 with $g = g_0 (\lambda/\lambda_0)^\alpha$ and approach 2 with $g = g_0$), where we consider a cloud scenario of a high optically thick cloud. Using the first approach the NUV and VIS windows provide little information on cloud parameters when the continuum is fitted with the wavelength-dependent scaling factor. Even in the NUV window with the prominent Ring features at the Ca II Fraunhofer lines the sensitivities are low for all cloud fractions: $C_{p_c} \leq 0.45$, $C_{f_c} \leq 0.25$ and $C_{\tau_c} \approx 0$. Furthermore

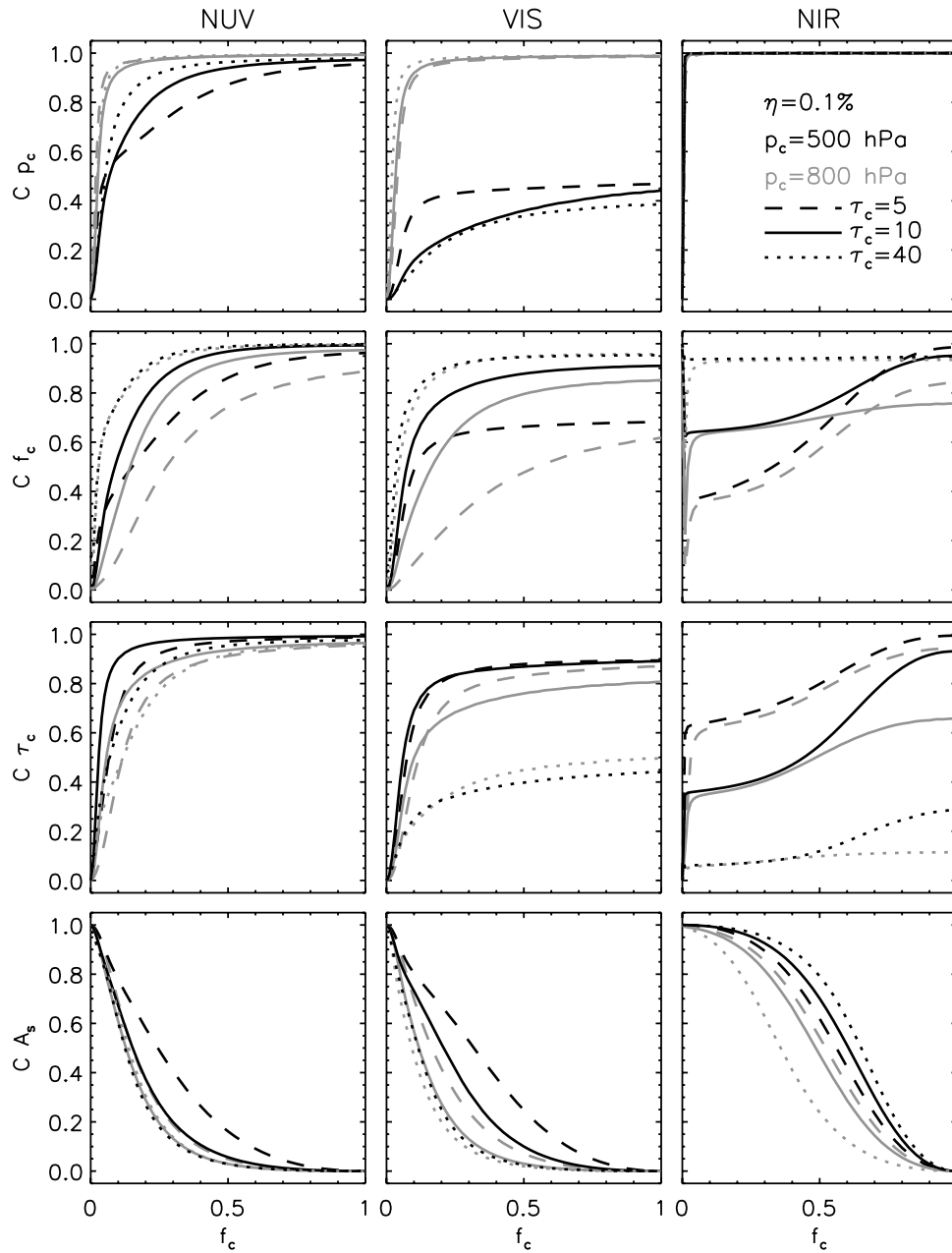


Figure 5. Retrieval sensitivities (C) to cloud top pressure (p_c), cloud fraction (f_c), cloud optical thickness (τ_c), and surface albedo (A_s) in the NUV, VIS, and NIR spectral windows as a function of cloud fraction for a fixed noise floor $\eta = 0.1\%$. Results are shown for the same cloud scenarios as in Figure 3. A surface albedo of 0.05 was used in all windows.

a small but significant amount of information on cloud top pressure and cloud fraction can be retrieved from the NUV Ring structures alone, but most of the cloud information of the NUV window comes from the spectral continuum.

[32] When the second approach is used, i.e., making use of the spectral signature of the continuum, the NUV window provides sufficient information on cloud top pressure and cloud fraction ($C_{p_c}, C_{f_c} \leq 0.9$ for $f_c \geq 0.2$), whereas for the VIS window only the cloud fraction can be retrieved with a reasonable sensitivity ($C_{f_c} \leq 0.9$ for $f_c > 0.2$). In contrast the NIR window shows a maximum sensitivity $C_{p_c} \approx 1$ for both types of scaling factor. Here the

information on cloud top pressure is extracted only from the relative spectral structures of the $O_2 A$ absorption features. Furthermore, cloud fraction can be retrieved with a reasonable sensitivity from NIR of about $C_{f_c} = 0.6 - 0.7$, which means that the cloud fraction is retrieved to a large extent from the relative $O_2 A$ absorption features. For all three windows the optical thickness cannot be retrieved if one of the two scaling factors is applied. The retrieval of surface albedo is also not possible for $f_c > 0.1$ because of fitting the two scaling factors (not shown in Figure 6). Thus, Figure 6 demonstrates that especially for the NUV and VIS window the continuum provides essential information on cloud

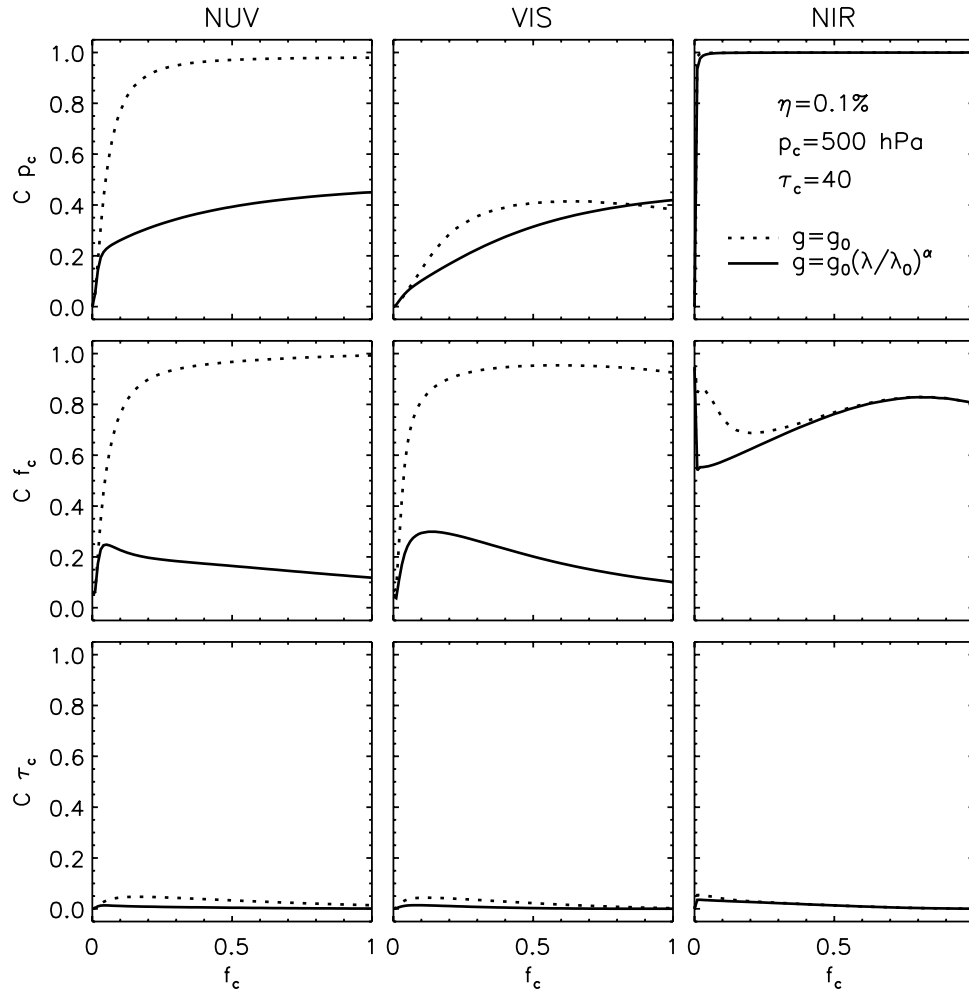


Figure 6. Retrieval sensitivities (C) to cloud top pressure (p_c), cloud fraction (f_c), and cloud optical thickness (τ_c) in the NUV, VIS, and NIR spectral windows when in addition to these parameters a power law (solid line, approach 1 in text) or a factor (dotted line, approach 2) is fitted to the reflectivity measurement. The retrieval sensitivities are shown as function of cloud fraction for $\eta = 0.1\%$, $p_c = 500$ hPa, and $\tau_c = 40$.

properties. Although the retrieval sensitivities in Figure 6 depend to some extent on the chosen cloud scenario the overall conclusions remain valid for the other cloud scenarios that are used in this study (not shown).

6. Synergistic Use of Spectral Windows

[33] Figure 5 showed that the NIR spectral window provides complementary information on cloud properties to the NUV and VIS spectral windows. The NIR window allows one to retrieve cloud top pressure with a high sensitivity C_{p_c} , whereas the NUV and VIS windows provide a higher sensitivity to τ_c . A combination of the NUV and NIR, or of the VIS and NIR window may improve the retrieval of cloud properties compared to a single window approach. *van Diedenhoven et al.* [2007] already showed that by using measurements in the wavelength range 350–390 nm in addition to O_2 A band measurements the sensitivity to cloud parameters can be significantly increased. In the following we investigate the retrieval capability of the combination of the NUV and NIR and of the

VIS and NIR reflectivity spectra. The state vector is extended to contain the surface albedo for each spectral window.

[34] Figure 7 shows the retrieval sensitivities for the combinations of spectral windows. The synergistic use of the NUV and NIR windows allows one to combine the ability to retrieve the three cloud parameters with high sensitivity. As a result, the three cloud parameters can be retrieved with maximum sensitivity $C_{p_c}, C_{f_c}, C_{\tau_c} \approx 1$ for nearly all cloud fractions. In other words one combines the ability of the NIR window to retrieve cloud top pressure for all possible cloud fractions with the ability of the NUV window to retrieve cloud fraction and cloud optical thickness with a high sensitivity. The combination of the VIS and NIR spectral range also improves the cloud retrieval compared to the single window approaches, but here the improvement is significantly less than for the NUV and NIR window combination. Especially the retrieval of cloud optical thickness for thick clouds is not sufficient with sensitivities $C_{\tau} < 0.5$ for cloud fractions smaller than 0.5. We also investigated the combination of the NUV and VIS

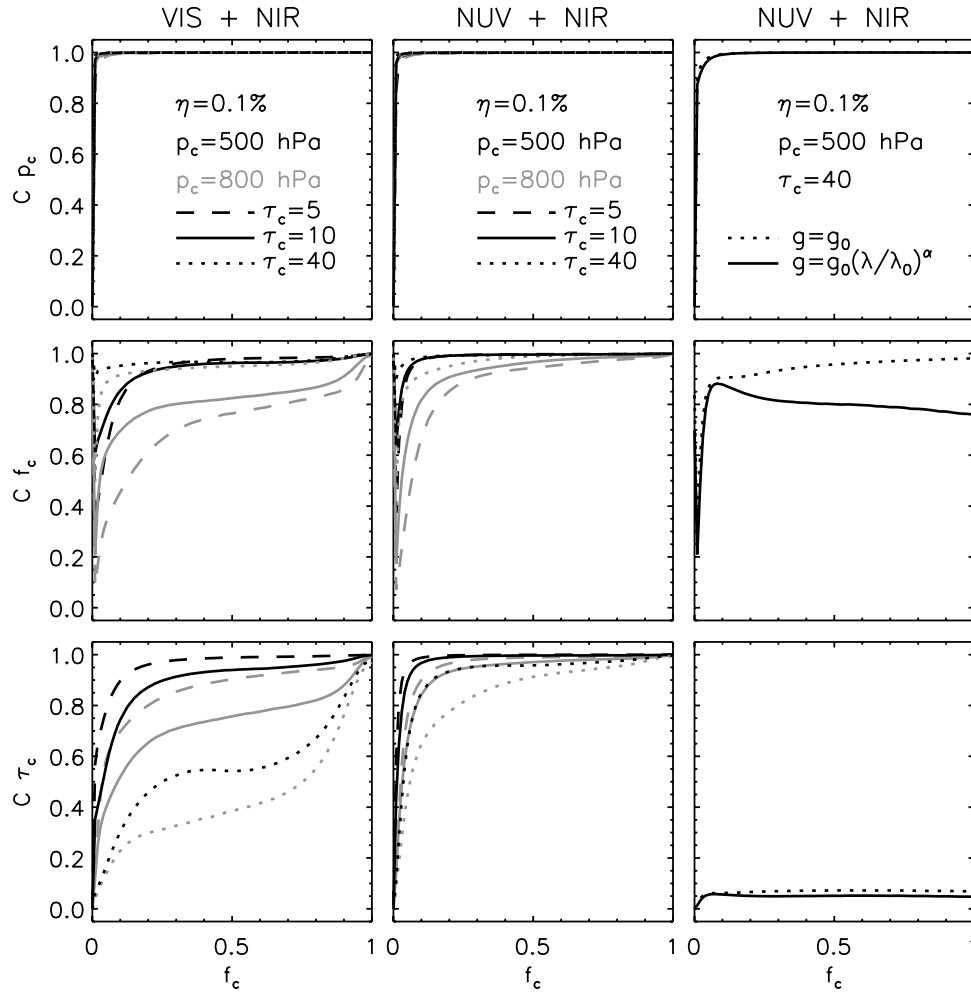


Figure 7. Retrieval sensitivities (C) to the cloud parameters p_c , f_c , and τ_c as a function of cloud fraction for the spectral window combination (left) VIS plus NIR and (middle) NUV plus NIR for a fixed noise floor $\eta = 0.1\%$. Results are shown for the four cloud scenarios of Figure 5. Also shown are retrieval sensitivities for the combination (right) NUV plus NIR when in addition to the cloud parameters a power law (solid line) or a factor (dotted line) is fitted to the reflectivity measurement in each window, using the same cloud scenario as in Figure 6.

windows and found no significant improvement for the retrieval of cloud properties compared to the NUV window alone (not shown). Since this spectral combination has no added value, it will not be considered in the remainder of this paper.

[35] In addition, the robustness of the fit with respect to random-like measurement biases is enhanced by the combination of spectral windows. Figure 8 shows the retrieval sensitivities for cloud parameters as a function of noise floor η . For the combination of the NUV and NIR spectral windows the sensitivities C_{p_c} , C_{f_c} , and C_{τ_c} larger than 0.9 in almost all cases. Only for the thick cloud C_{τ_c} reduces to values between 0.7 and 0.9 for a noise floor $\eta \geq 1\%$. A high robustness is also achieved for the combination of the VIS and NIR windows. However, the retrieval of cloud optical thickness is more sensitive to the noise floor than for the NUV + NIR combination.

[36] The third column of Figure 7 presents retrieval simulations of the combined NUV and NIR windows when in addition to the cloud parameters the power law scaling

factor is fitted to the spectra in each window. When the wavelength-dependent scaling factor is fitted to the spectrum (g_0 and α added to the state vector for each spectral window), the combination of the NUV and NIR measurements does not contain significantly more information than only measurements in the NIR window. This can be explained by our previous finding that the extra information of the NUV with respect to the NIR retrieval originates from the continuum signature of the NUV window. However, the NIR retrieval can be improved by the synergistic use of both spectral windows when only a wavelength-independent scaling factor is fitted to the spectrum (only g_0 added to state vector for each window). We can then retrieve the cloud fraction f_c with a maximum sensitivity $C_f \approx 1$ for nearly all cloud fractions.

[37] Furthermore, we found that for the combination of the NUV and NIR spectral windows the Ring effect does not significantly contribute to the retrieval of cloud parameters. To demonstrate this we replaced the NUV reflectivity spectrum with a NUV reflectivity spectrum where we did

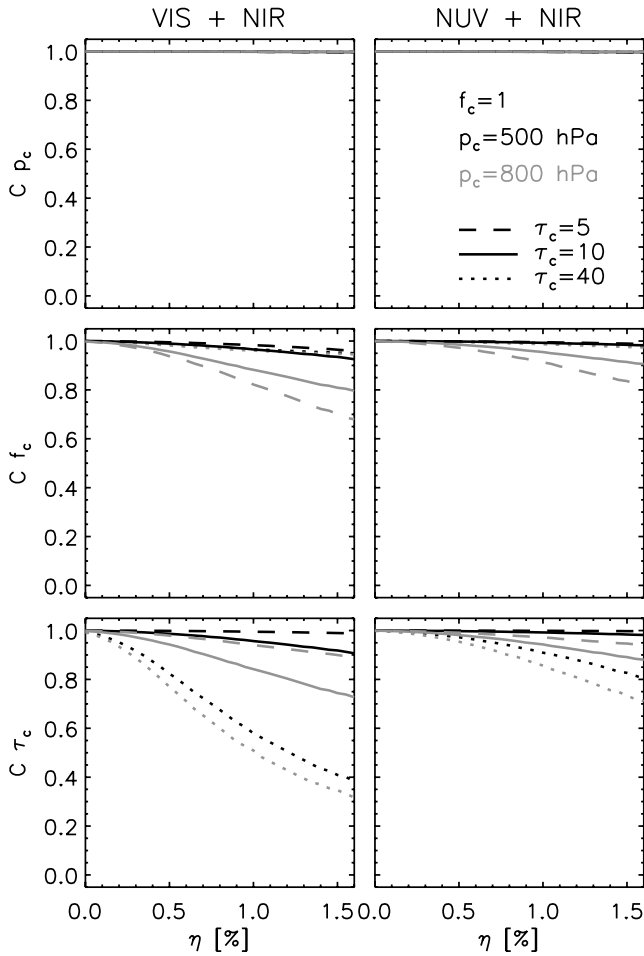


Figure 8. Same as Figure 3 but for the spectral window combinations VIS plus NIR and NUV plus NIR.

not take inelastic Raman scattering into account. This modification of the measurement simulation hardly affected the retrieval sensitivity. The loss of sensitivity of the NUV measurement with respect to cloud top pressure is completely compensated by the sensitivity of the $O_2 A$ absorption band in the NIR measurement. For the design of a future instrument this means that the spectral resolution requirement on the NUV measurements can be relaxed, because it is not needed to resolve the spectrally fine Ring effect features in the spectrum. Furthermore, our results implicate that it allows one to simulate the Ring effect on the spectrum with a precalculated Ring spectrum and certain fudge parameters, such as an amplitude of the Ring spectrum, to account for the different strength of the Ring effect depending on the atmospheric state. This commonly used approach [e.g., *Chance, 1998*] eases the time-consuming radiative transfer calculations that include inelastic Raman scattering considerably.

[38] Overall, the combination of the NUV and NIR window is superior to the combination of the VIS and NIR spectral range. It improves the NIR and NUV cloud retrieval significantly so that all three cloud parameters; that is, cloud top pressure, cloud fraction and cloud optical thickness can be retrieved from the measurement with a high robustness to random-like measurement biases. This

added value compared to a single NIR window approach originates from the spectral shape of the continuum in the NUV window. The relative Ring structures do not provide significant extra information in this combination. This means that the maximum benefit of the synergistic use of both spectral windows can only be achieved when the broadband spectral features are exploited in the spectrum. Therefore, the broadband radiometric calibration of the NUV requires special attention for the retrieval of cloud properties.

7. Implication for Tropospheric NO_2 Column Retrievals

[39] The retrieval of cloud parameters from NUV, VIS, and NIR spectral ranges is used to support trace gas retrieval. In this section, we demonstrate the effect of cloud retrieval errors on the retrieval of tropospheric NO_2 columns. Tropospheric NO_2 column densities from GOME and its successors have gained important insight into the source strength of mainly anthropogenic NO_x emissions [e.g., *Beirle et al., 2003; Richter et al., 2005*]. These retrievals are very sensitive to the presence of clouds, since most tropospheric NO_2 resides below the cloud [e.g., *Boersma et al., 2004; Wang et al., 2006*].

[40] The DOAS technique is commonly used to derive NO_2 columns from reflectivity measurements in the spectral range 420–450 nm. This technique separates the reflectivity spectrum into a spectrally smooth part and a differential absorption feature. From the differential spectral structure a slant gas column N_s is derived. This slant column is converted to the vertical column N_v via

$$N_v = N_s/M, \quad (17)$$

where M is the so-called NO_2 air mass factor given by

$$M = \frac{-\ln(r/r_0)}{\tau_{NO_2}}. \quad (18)$$

Here, r is the reflectivity at 440 nm with NO_2 absorption included, r_0 is the reflectivity at 440 nm without NO_2 absorption in the model atmosphere, and τ_{NO_2} is the total NO_2 absorption optical thickness.

[41] Because of equation (17) the error on the vertical NO_2 column imposed by errors in the derived cloud parameters is the same as the relative error on the air mass factor M . The latter can be calculated in a straightforward manner using

$$e_M = \frac{1}{M} \sqrt{\mathbf{k}^T \mathbf{S} \mathbf{k}}. \quad (19)$$

Here, \mathbf{S} is the total error covariance matrix from equation (14) and vector \mathbf{k} describes the sensitivity of the air mass factor M to the cloud parameters x_i , namely,

$$k_i = \frac{\partial M}{\partial x_i}. \quad (20)$$

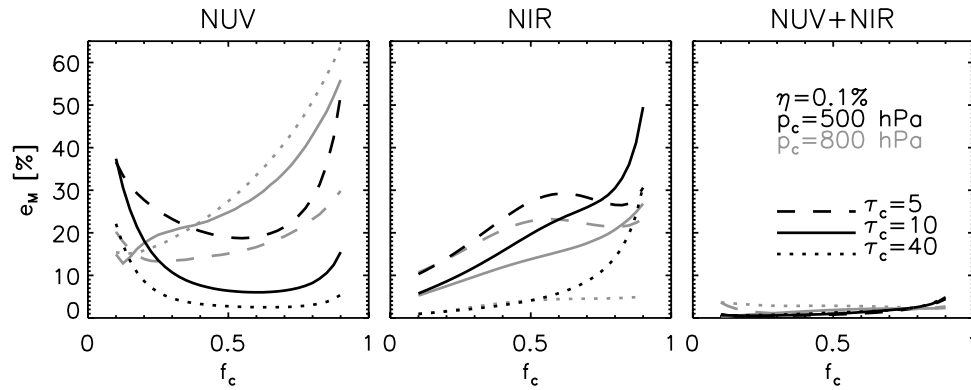


Figure 9. Error e_M on the tropospheric NO_2 air mass factor as a result of errors on retrieved cloud parameters from spectral windows NUV, NIR, and the combination NUV plus NIR. The error is shown as a function of cloud fraction for the same scenarios as in Figures 4 and 7.

[42] To simulate the error on the tropospheric air mass factor, e_M , we assume the same model atmosphere as described in section 2, but adopt the NO_2 density profile from Wang *et al.* [2006]. This NO_2 density profile corresponds to a polluted scene with 2.3 ppbv NO_2 in the lowest 2 km and no NO_2 at higher altitudes.

[43] To determine the error covariance matrix \mathbf{S} the a priori covariance matrix \mathbf{S}_a is needed. Because of the strong variability of clouds in space and time it is difficult to get a realistic estimate of \mathbf{S}_a . For the purpose of this study we assume uncorrelated a priori errors with $e_{A_s} = 0.01$, $e_{f_c} = 0.3$, $e_{\tau_c} = 5$, and $e_{p_c} = 300$ hPa, which represents a relatively large uncertainty of the a priori estimate.

[44] Figure 9 shows the error of the tropospheric NO_2 air mass factor, e_M , as a function of cloud fraction. Here, cloud parameters are retrieved from reflectivity measurements in the NUV and NIR window, and from the combination of both windows. The relative error e_M increases when the cloud fraction increases, both for the NUV and the NIR cloud retrieval. This dependence is caused by two effects: Firstly, for increasing cloud fractions both the sensitivity of the air mass factor and the error e_M with respect to cloud parameters increase. Secondly, for cloud fractions close to 1 nearly all tropospheric NO_2 is shielded by the cloud. This means that the NO_2 air masses are smaller at these fractions, and in turn, the relative error e_M increases significantly for these cloud fractions.

[45] For the NUV window retrieval and the high-cloud case scenario, the error on the air mass factor also increases at smaller cloud fractions. This feature can be explained by the retrieval sensitivities for the NUV retrieval as shown in Figure 5. For low-cloud fractions the retrieval sensitivity C_{p_c} for cloud top pressure is much lower for the high-cloud scenario than for the low-cloud scenario. Hence, the a priori error on cloud top height has a stronger impact on the total error for the high cloud than for the low cloud, which explains the corresponding increase of e_M for small cloud fractions. Because of the larger retrieval sensitivity, this effect cannot be observed for the NIR window retrieval. This is mainly due to the characteristic retrieval sensitivity to cloud top pressure of the O_2 A band that is high even for very low cloud fractions (see Figure 5).

[46] Clearly, the combination of the NUV and NIR windows provides a superior retrieval result compared to using the windows separately. In this case the error e_M is less than 5%. Similar values for e_M were found by van Diedenhoven *et al.* [2007] for this combination of spectral windows. The significantly smaller errors are due to the higher information content when the NUV and NIR windows are used. Using this combination minimizes the biases due to the a priori errors.

8. Summary and Conclusion

[47] The majority of satellite-based reflectivity measurements are affected by clouds. To enable trace gas retrievals for cloudy scenes it is essential to retrieve auxiliary parameters that adequately describe the clouds. Our purpose was to find out which spectral window or which combination of windows is most suited to retrieve this cloud information for present and future GOME-type instruments. We compared the retrieval of cloud top pressure, cloud fraction, cloud optical thickness and surface albedo from three spectral windows that are currently used for this purpose: (1) the NUV window (350–400 nm), which contains pronounced Ring effect structures, (2) the VIS window (460–490 nm), which contains an O_2 - O_2 band, and (3) the NIR window (755–775 nm) that contains the O_2 A band.

[48] Using the spectral windows separately we found that the VIS window provides the least information on cloud properties. The retrieval capability of this window is especially limited in the case of high and optically thick clouds. We found that the retrieval of cloud top pressure and cloud optical thickness from these measurements is very sensitive to random-like spectral biases on the reflectivity measurement. Since a significant amount of the cloud parameter information originates from the spectral continuum, the radiometric calibration limits the measurement interpretation. In all cases, the surface albedo in each window could only be retrieved for low-cloud fractions.

[49] The NIR window is most capable of retrieving cloud top pressure. The strong O_2 A absorption feature in this window yields a high robustness to random-like biases. However, information on cloud optical thickness, which originates predominantly from the spectral continuum, is easily lost when random-like spectral biases increase. An-

other important aspect of the retrieval of cloud parameters from this window is that it is still possible to retrieve cloud top pressure with high retrieval sensitivity without using the cloud information contained in the spectral continuum, in contrast to the other windows. To a large extent this is also the case for the retrieval of cloud fraction. Thus, the NIR window allows one to retrieve cloud top pressure even when the measurement is subject to large spectrally broad calibration errors, but retrieval of the other cloud parameters proves to be problematic.

[50] Retrievals from NUV measurements show a retrieval sensitivity close to one for cloud fractions $f_c > 0.4$ for all three cloud parameters but this information decreases rapidly for smaller cloud fractions. Furthermore, the retrieval from the NUV window is sensitive to random-like biases on the measurements. Nevertheless, even for a noise floor of 0.5% a reasonable performance is obtained. In this spectral window the cloud information is mainly extracted from the spectral continuum. Additionally, the Ring effect provides a small but significant contribution to the retrieval of cloud top pressure. When the relative spectral dependence of the continuum but not its absolute value is used cloud top pressure and cloud fraction can be retrieved adequately, but information is lost on cloud optical thickness.

[51] Because of the different performance of cloud retrieval from the NUV and NIR window a superior single window approach cannot be appointed. Both windows provide, to a certain extent, complementary information, which can be best exploited when both windows are used in a synergistic manner in a cloud retrieval as was proposed by van Diedenhoven et al. [2007]. We have shown in this study that errors on retrieved NO_2 columns can be significantly reduced when the combination of the NUV and NIR spectral windows is used. The absolute continuum height and relative spectral dependence in the NUV window aid the retrieval of cloud fraction and cloud optical thickness, which are difficult to determine simultaneously from the NIR window continuum alone. We found that the Ring effect structures do not significantly contribute in this combination of the NUV and NIR window in terms of information content on cloud top pressure, cloud fraction, and cloud optical thickness. This means that for future instruments the requirement on the instrument spectral resolution of the NUV window to resolve the Ring effect structures can be relaxed for the purpose of cloud retrieval, because the Ring features do not have to be resolved when the NUV and NIR window are combined. Furthermore, this allows one to simplify the radiative transfer modeling in the NUV considerably, and thus, eases the setup of an efficient retrieval approach.

[52] Finally, for GOME(-2), SCIAMACHY and similar instruments in the future we propose to retrieve cloud parameters from the NUV and NIR window combined. For OMI-type instruments that lack the NIR spectral window we propose to use the NUV window including the Ring structures, which has the potential to retrieve all cloud parameters, i.e., cloud pressure, cloud fraction and cloud optical thickness for cloud fractions larger than 0.4. However, because of the sensitivity of the retrieval to an additional noise floor on the measurement, but also because of the importance to use the spectral continuum in the NUV

window, an accurate calibration of the measurement is crucial for this type of cloud parameter retrieval.

References

- Acarreta, J. R., J. F. De Haan, and P. Stammes (2004), Cloud pressure retrieval using the $\text{O}_2\text{-O}_2$ absorption band at 477 nm, *J. Geophys. Res.*, *109*, D05204, doi:10.1029/2003JD003915.
- Ahmad, Z., P. K. Bhartia, and N. Krotkov (2004), Spectral properties of backscattered UV radiation in cloudy atmospheres, *J. Geophys. Res.*, *109*, D01201, doi:10.1029/2003JD003395.
- Bates, D. R. (1984), Rayleigh scattering by air, *Planet. Space. Sci.*, *32*, 785–790.
- Beirle, S., U. Platt, M. Weing, and T. Wagner (2003), Weekly cycle of NO_2 by GOME measurements: A signature of anthropogenic sources, *Atmos. Chem. Phys.*, *3*, 2225–2232.
- Boersma, K. F., H. J. Eskes, and E. J. Brinksma (2004), Error analysis for tropospheric NO_2 retrieval from space, *J. Geophys. Res.*, *109*, D04311, doi:10.1029/2003JD003962.
- Bovensmann, H., J. Burrows, M. Buchwitz, J. Frerick, S. Noël, V. Rozanov, K. Chance, and A. Goede (1999), SCIAMACHY: Mission objectives and measurement modes, *J. Atmos. Sci.*, *56*, 127–150.
- Bucholtz, A. (1995), Rayleigh scattering calculations for the terrestrial atmosphere, *Appl. Opt.*, *34*, 2765–2773.
- Burrows, J. P., A. Dehn, B. Deters, S. Himmelman, A. Richter, S. Voigt, and J. Orphal (1999a), Atmospheric remote-sensing reference data from GOME: 2. Temperature-dependent absorption cross sections of O_3 in the 231–794 nm range, *J. Quant. Spectrosc. Radiat. Transfer*, *61*, 509–517.
- Burrows, J. P., et al. (1999b), The Global Ozone Monitoring Experiment (GOME): Mission concept and first scientific results, *J. Atmos. Sci.*, *56*, 151–175.
- Callies, J. E., E. Corpaccioli, M. Eisinger, A. Hahne, and A. Lefebvre (2000), GOME-2—Metop's second-generation sensor for operational ozone monitoring, *ESA Bull.*, *102*, 28–36.
- Chance, K. (1998), Analysis of BrO measurements from the Global Ozone Monitoring Experiment, *Geophys. Res. Lett.*, *25*, 3335–3338.
- Chance, K., and R. J. D. Spurr (1997), Ring effect studies: Rayleigh scattering, including molecular parameters for rotational Raman scattering, and the Fraunhofer spectrum, *Appl. Opt.*, *36*, 5224–5230.
- Daniel, J. S., S. Solomon, H. L. Miller, A. O. Langford, R. W. Portmann, and C. S. Eubank (2003), Retrieving cloud information from passive measurements of solar radiation absorbed by molecular oxygen and $\text{O}_2\text{-O}_2$, *J. Geophys. Res.*, *108*(D16), 4515, doi:10.1029/2002JD002994.
- de Beek, R., M. Vountas, V. V. Rozanov, A. Richter, and J. P. Burrows (2001), The Ring effect in the cloudy atmosphere, *Geophys. Res. Lett.*, *28*, 721–724.
- Grainger, J. F., and J. Ring (1962), Anomalous Fraunhofer line profiles, *Nature*, *193*, 762.
- Greenblatt, G. D., J. J. Orlando, J. B. Burkholder, and A. R. Ravishankara (1990), Absorption measurements of oxygen between 330 and 1140 nm, *J. Geophys. Res.*, *95*, 18,577–18,582.
- Hansen, P. (1992), Analysis of discrete ill posed problems by means of the L-curve, *SIAM Rev.*, *34*, 561–580.
- Hansen, P., and D. O'Leary (1993), The use of the L-curve in the regularization of discrete ill posed problems, *SIAM J. Sci. Comput.*, *14*, 1487–1503.
- Hasekamp, O. P., and J. Landgraf (2005), Retrieval of aerosol properties over the ocean from multispectral single-viewing-angle measurements of intensity and polarization: Retrieval approach, information content, and sensitivity study, *J. Geophys. Res.*, *110*, D20207, doi:10.1029/2005JD006212.
- Joiner, J., and A. P. Vasilkov (2006), First results from the OMI rotational Raman scattering cloud pressure algorithm, *IEEE Trans. Geosci. Remote Sens.*, *44*, 1272–1282.
- Joiner, J., P. K. Bhartia, R. P. Cebula, E. Hilsenrath, R. D. McPeters, and H. Park (1995), Rotational Raman scattering (Ring effect) in satellite backscatter ultraviolet measurements, *Appl. Opt.*, *34*, 4513–4525.
- Joiner, J., A. P. Vasilkov, D. E. Flittner, J. F. Gleason, and P. K. Bhartia (2004), Retrieval of cloud pressure and oceanic chlorophyll content using Raman scattering in GOME ultraviolet spectra, *J. Geophys. Res.*, *109*, D01109, doi:10.1029/2003JD003698.
- Koелеmeijer, R. B. A., and P. Stammes (1999), Validation of Global Ozone Monitoring Experiment cloud fractions relevant for accurate ozone column retrieval, *J. Geophys. Res.*, *104*, 18,801–18,814.
- Koелеmeijer, R. B. A., P. Stammes, J. W. Hovenier, and J. F. de Haan (2001), A fast method for retrieval of cloud parameters using oxygen A band measurements from the Global Ozone Monitoring Experiment, *J. Geophys. Res.*, *106*, 3475–3490.
- Kokhanovsky, A. A., V. V. Rozanov, E. P. Zege, H. Bovensmann, and J. P. Burrows (2003), A semianalytical cloud retrieval algorithm using back-

- scattered radiation in 0.4–2.4 μm spectral region, *J. Geophys. Res.*, 108(D1), 4008, doi:10.1029/2001JD001543.
- Krijger, J. M., M. van Weele, I. Aben, and R. Frey (2007), The effect of sensor resolution on the number of cloud-free observations from space, *Atmos. Chem. Phys.*, 7, 2881–2891.
- Kuze, A., and K. Chance (1994), Analysis of cloud top height and cloud coverage from satellites using the O₂ A and B bands, *J. Geophys. Res.*, 99, 14,481–14,491.
- Landgraf, J., O. P. Hasekamp, R. van Deelen, and I. Aben (2004), Rotational Raman scattering of polarized light in the Earth's atmosphere: A vector radiative transfer model using the radiative transfer perturbation theory approach, *J. Quant. Spectrosc. Radiat. Transfer*, 87, 399–433.
- Levelt, P. F., G. H. J. van den Oord, M. R. Dobber, A. Mälkki, H. Visser, J. de Vries, P. Stammes, J. O. V. Lundell, and H. Saari (2006), Ozone Monitoring Instrument, *IEEE Trans. Geosci. Remote Sens.*, 44, 1093–1101.
- Liu, X., M. J. Newchurch, R. Loughman, and P. K. Bhartia (2004), Errors resulting from assuming opaque Lambertian clouds in TOMS ozone retrieval, *J. Quant. Spectrosc. Radiat. Transfer*, 85, 337–365.
- Marshak, A., L. Oreopoulos, A. B. Davis, W. J. Wiscombe, and R. F. Calahan (1999), Errors induced by the neglect of polarization in radiance calculations for Rayleigh-scattering atmospheres, *Geophys. Res. Lett.*, 26, 1585–1588.
- Peck, E. R., and D. J. Fisher (1964), Dispersion of argon, *J. Opt. Soc. Am.*, 54, 1362–1364.
- Penney, C. M., R. L. St. Peters, and M. Lapp (1974), Absolute rotational Raman cross sections for N₂, O₂, and CO₂, *J. Opt. Soc. Am.*, 64, 712–716.
- Phillips, P. (1962), A technique for the numerical solution of certain integral equations of the first kind, *J. Assoc. Comput. Mach.*, 9, 84–97.
- Platt, U. (1994), Differential optical absorption spectroscopy (DOAS), in *Air Monitoring by Spectroscopic Techniques*, Chem. Anal. Ser., vol. 127, edited by M. W. Sigrist, pp. 27–84, John Wiley, New York.
- Richter, A., J. P. Burrows, H. Nüß, C. Granier, and U. Niemeier (2005), Increase in tropospheric nitrogen dioxide over China observed from space, *Nature*, 437, 129–132, doi:10.1038/nature04092.
- Rodgers, C. (2000), *Inverse Methods for Atmospheric Sounding, Theory and Practice*, World Sci., Singapore.
- Rothman, L. S., et al. (2005), The HITRAN 2004 molecular spectroscopic database, *J. Quant. Spectrosc. Radiat. Transfer*, 96, 139–204.
- Sioris, C. E., and W. F. J. Evans (2000), Impact of rotational Raman scattering in the O₂ A band, *Geophys. Res. Lett.*, 27, 4085–4088.
- Stam, D. M., I. Aben, and F. Helderma (2002), Skylight polarization spectra: Numerical simulation of the Ring effect, *J. Geophys. Res.*, 107(D20), 4419, doi:10.1029/2001JD000951.
- Tikhonov, A. (1963), On the solution of incorrectly stated problems and a method of regularization, *Dokl. Akad. Nauk SSSR*, 151, 501–504.
- Tran, H., C. Boulet, and J.-M. Hartmann (2006), Line mixing and collision-induced absorption by oxygen in the A band: Laboratory measurements, model, and tools for atmospheric spectra computations, *J. Geophys. Res.*, 111, D15210, doi:10.1029/2005JD006869.
- Vandaele, A. C., C. Hermans, P. C. Simon, M. Carleer, R. Collin, S. Fally, M. F. Mérienne, A. Jenouvrier, and B. Coquart (1998), Measurements of the NO₂ absorption cross-section from 42000 cm⁻¹ to 10000 cm⁻¹ (238–1000 nm) at 220 K and 294 K, *J. Quant. Spectrosc. Radiat. Transfer*, 59, 171–184.
- van Deelen, R., O. P. Hasekamp, and J. Landgraf (2007), Accurate modeling of spectral fine-structure in Earth radiance spectra measured with the Global Ozone Monitoring Experiment, *Appl. Opt.*, 46, 243–252.
- van Dierenhoven, B., O. P. Hasekamp, and J. Landgraf (2006), Efficient vector radiative transfer calculations in vertically inhomogeneous cloudy atmospheres, *Appl. Opt.*, 45, 5993–6006.
- van Dierenhoven, B., O. P. Hasekamp, and J. Landgraf (2007), Retrieval of cloud parameters from satellite-based reflectance measurements in the ultraviolet and the oxygen A-band, *J. Geophys. Res.*, 112, D15208, doi:10.1029/2006JD008155.
- Wang, P., P. Stammes, and F. Boersma (2006), Impact of the effective cloud fraction assumption on tropospheric NO₂ retrievals, in *Proceedings of the First Atmospheric Science Conference, Frascati, Italy*, edited by H. Lacoste, *Eur. Space Agency Spec. Publ.*, ESA SP-628, 4–38.
- Yang, Z., P. O. Wennberg, R. P. Cageao, T. J. Pongetti, G. C. Toon, and S. P. Sander (2005), Ground-based photon path measurements from solar absorption spectra of the O₂ A band, *J. Quant. Spectrosc. Radiat. Transfer*, 90, 309–321.

O. P. Hasekamp, J. Landgraf, R. van Deelen, and B. van Dierenhoven, Netherlands Institute for Space Research, Sorbonnelaan 2, NL-3584 CA Utrecht, Netherlands. (r.van.deelen@gmail.com)